Earth and Planetary Science Letters 419 (2015) 101–110

Contents lists available at ScienceDirect

Earth and Planetary Science Letters

www.elsevier.com/locate/epsl

Regional temperature, atmospheric circulation, and sea-ice variability within the Younger Dryas Event constrained using a speleothem from northern Iberia

Lisa M. Baldini [a,*], Frank McDermott [b,c], James U.L. Baldini [a], Pablo Arias [d], Marián Cueto [d], Ian J. Fairchild [e], Dirk L. Hoffmann [f,g], David P. Mattey [h], Wolfgang Müller [h], Dan Constantin Nita [f], Roberto Ontañón [d], Cristina Garciá-Moncó [d], David A. Richards [f]

[a] Department of Earth Sciences, Durham University, Science Labs, South Road, Durham DH1 3LE, UK
[b] UCD School of Geological Sciences, University College Dublin, Belfield, Dublin 4, Ireland
[c] UCD Earth Institute, University College Dublin, Belfield, Dublin 4, Ireland
[d] International Institute for Prehistoric Research of Cantabria, University of Cantabria, Spain
[e] School of Geography, Earth and Environmental Sciences, University of Birmingham, Edgbaston, Birmingham B15 2TT, UK
[f] School of Geographical Sciences, University of Bristol, University Road, Clifton, Bristol BS8 1SS, UK
[g] CENIEH, Paseo Sierra de Atapuerca s/n, 09002 Burgos, Spain
[h] Department of Earth Sciences, Royal Holloway, University of London, Egham, Surrey, TW20 0EX, UK

ARTICLE INFO

Article history:
Received 4 September 2014
Received in revised form 5 March 2015
Accepted 5 March 2015
Available online 25 March 2015
Editor: G.M. Henderson

Keywords:
Younger Dryas
isotopes
NAO
westerlies
stalagmite
trace elements

ABSTRACT

Precisely-dated, high-resolution stable isotope and trace element data from a stalagmite from La Garma Cave, northern Spain, reveal several stages of distinct climatic variability along the northern Iberian Atlantic margin, and provide new constraints on the latitude of North Atlantic westerlies during the Younger Dryas Event (YD). Westerly wind position (reconstructed using sub-annually resolved Mg data as a proxy for sea spray contributions associated with wind strength at this coastal cave site) during the early YD (12.85–12.15 kyr) oscillated meridionally, resembling the decadal-scale component of the modern North Atlantic Oscillation (NAO). Northward repositioning of westerly storm tracks over northern Iberia began at ∼12.15 kyr, consistent with other high-resolution wind proxy reconstructions from central and northern Europe, but occurred more gradually nearer the Atlantic margin. From ∼12.15 kyr to the YD termination, atmospheric circulation resembled a persistently positive NAO, with westerlies reaching their maximum northward extent at 11.8 kyr (reflected by a Mg concentration minimum at this time). Air temperature (reflected by our $\delta^{18}O$ data) and Iberian wind strength were predominantly coupled throughout the YD suggesting that temperature modulated sea-ice extent, and consequently controlled westerly wind latitude. However our data suggest that abrupt warming at 12.1 kyr was followed by much more gradual northward shifts in westerly position, and that a lag existed between the warming and sea-ice retreat. This gradual return of the westerlies to the north beginning at 12.1 kyr is consistent with inferred changes in wind strength at other European sites. Additionally, atmospheric circulation inferred from our northern Iberian wind strength proxy record generally tracked low-frequency meridional shifts in Intertropical Convergence Zone position, corroborating past research that suggested closely coupled low- and high-latitude atmospheric teleconnections over this period.

1. Introduction

The Younger Dryas Event (YD; 12.846 to 11.653 kyr based on NGRIP chronology (GICC05) (Rasmussen et al., 2006); kyr = kilo-year BP 1950) is the most extensively studied abrupt climate event over the whole of the last glacial cycle, but its cause and internal structure are still debated. A catastrophic outburst of proglacial lake meltwater associated with the retreating Laurentide Ice Sheet that consequently slowed Atlantic meridional overturning circulation (AMOC) is most often invoked to explain the YD (Broecker, 2006; Broecker et al., 1989; Carlson et al., 2007), although other causes have been proposed, including a bolide impact (Firestone et al., 2007; Kennett et al., 2009). The YD was historically considered

* Corresponding author.
E-mail address: l.m.baldini@durham.ac.uk (L.M. Baldini).

http://dx.doi.org/10.1016/j.epsl.2015.03.015
0012-821X/

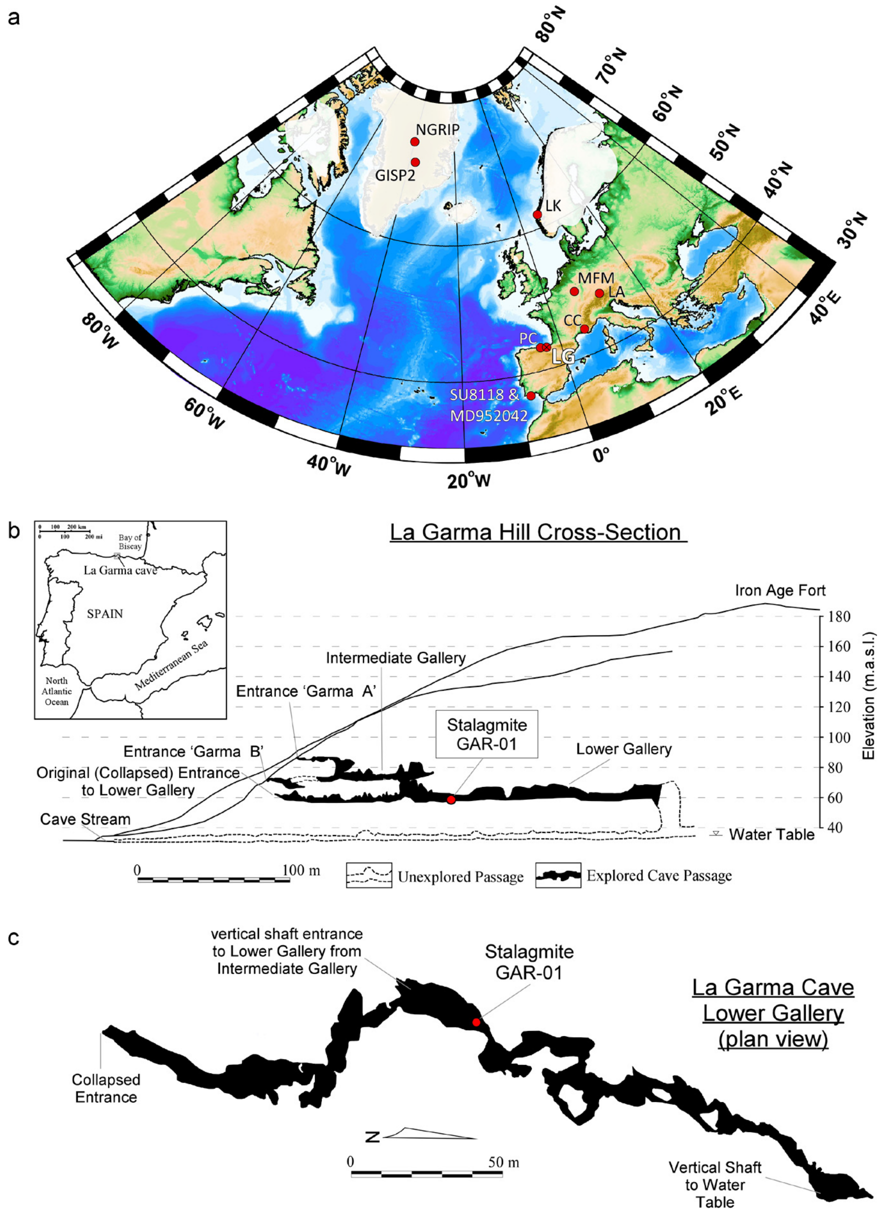

Fig. 1. (a) Locations of YD palaeoclimate archive sites along the North Atlantic margin discussed in the text. Large continental glaciers are represented by the semi-transparent white areas. Glacier extent is based on several recent publications (O'Cofaigh et al., 2013; Young et al., 2012) but probably represents a minimum extent because limited evidence is preserved for YD ice extent on shelves, particularly around Greenland (O'Cofaigh et al., 2013). LG, La Garma Cave; MFM, Meerfelder Maar; LA, Lake Ammersee; PC, El Pindal Cave; LK, Lake Kråkenes; CC, Chauvet Cave; SU8118 & MD952042, Iberian margin sediment cores; NGRIP, North GRIP ice core; GISP2, GISP2 ice core. (b) Location of La Garma Cave in northern Spain and cave cross section and (c) plan of the main levels of the karst system (Arias and Ontañón, 2012). Stalagmite GAR-01 was obtained from the Lower Gallery. The position of the sample is represented by a red filled circle. (For interpretation of the references to colour in this figure legend, the reader is referred to the web version of this article.)

to be an event characterised by a return to near glacial conditions, but recent research indicates that colder conditions were restricted to the Northern Hemisphere, and that the Southern Hemisphere actually warmed (Shakun and Carlson, 2010). Recently, attention has focussed on constraining possible large-scale atmospheric shifts within the YD. Lake sediment records from Norway (Lake Kråkenes: LK) and Germany (Meerfelder Maar: MFM) indicate atmospheric circulation changes occurred, with a dramatic climatic amelioration approximately mid-way through the YD at the so-called '12.15 kyr event'. These studies suggest that sea-ice variability during the YD could have caused switching of the meridional position of the North Atlantic westerlies (Bakke et al., 2009; Brauer et al., 2008). Thus, it has been argued that during the early YD (prior to 12.15 kyr), southward expansion of North Atlantic sea ice may have steered westerlies in a more zonal path over central Europe and MFM, whereas during the late YD (after 12.15 kyr), sea-ice breakup redirected the westerlies northwards towards LK. The high-resolution records from the same two sites were used in a subsequent study to suggest that warming associated with the 12.15 kyr event was locally abrupt, but occurred at different times in different locations, and may relate to the gradual northward migration of the Polar Front (Lane et al., 2013). However, these records are located away from the North Atlantic, and no similarly high-resolution record exists proximal to the North Atlantic seaboard to characterise westerly migration test of these interpretations.

Here we present geochemical records from a speleothem from La Garma Cave in northern Spain that constrain regional temperature and local wind strength shifts during the YD at a subannual resolution. The cave is set in a maritime climate that is strongly sensitive to the NAO (Gouveia et al., 2008) (i.e. the modern control on the position of the North Atlantic westerlies), AMOC strength (Pohlmann et al., 2006), and, through teleconnections, to the position of the Intertropical Convergence Zone (ITCZ) (Souza and Cavalcanti, 2009). During the YD, this region also marked the southern boundary of the Polar Front (Ruddiman and Mcintyre, 1981). The site is therefore ideally situated for clarifying the complex interplay between possible AMOC weakening, sea-ice growth, and the basin-wide atmospheric response.

2. Site description

La Garma Cave (43°25′N, 3°40′W) is located 12 km ESE of Santander and 5 km inland from the Bay of Biscay in the northern Spanish province of Cantabria at an elevation of 85 m.a.s.l. The cave was discovered in 1995 at which time a detailed survey was conducted and gates erected to restrict access via the two modern cave entrances, Garma A and Garma B (Fig. 1). Detailed archaeological investigations of the cave, conducted by P. Arias and co-researchers at the University of Cantabria, are ongoing.

Developed in lower Cretaceous limestone on seven main levels within a 187 m high hill, La Garma Cave contains ten principal archaeological sites (Arias and Ontañón, 2012), the most important of which are located in the levels at 59 and 80 m.a.s.l. (the Lower Gallery and La Garma A, respectively) (Fig. 1). The former is a 300 m long passage, whose original entrance was blocked by rockfall in the Pleistocene. This rockfall abruptly isolated a Palaeolithic (16.5 kyr) site within this passage (Supplemental Fig. S1), thus preserving the remains of the activity of its last occupants, including dwelling structures and ritual areas directly observable without excavation (Arias, 2009; Arias and Ontañón, 2012). The site's Upper Palaeolithic archaeology is important, with a very high density of well-preserved material scattered across approximately 800 m^2 of cave floor. Stalagmite GAR-01 was deposited on top of these Upper Palaeolithic floors in the Lower Gallery. The gallery also has an important ensemble of Palaeolithic cave art representing several different cultural periods, and was used as a burial cave during the Middle Ages (∼1.3 kyr). In 2008, La Garma Cave was included in the UNESCO World Heritage List.

Vegetation above the cave consists of dense C3 vegetation, including hazel, bay and eucalyptus (Rudzka-Phillips et al., 2013). Soil depth varies, but is typically about one meter. The mean annual temperature at the site is 13.7 °C, the mean annual total rainfall is 1278 mm yr^{-1}, with a mean annual water excess (total rainfall – actual evapotranspiration) of 1090 mm yr^{-1} (Rudzka-Phillips et al., 2013). The relevant results of La Garma Cave modern-day monitoring conducted from 2004 to 2005 are presented in the Supplementary Material.

3. Methods

3.1. Sample GAR-01 description and preparation

Stalagmite GAR-01 was collected in 2004 from the Lower Gallery in La Garma Cave (Fig. 1) and is composed entirely of dense, white columnar crystalline calcite (see Supplementary Material for additional information). An unusual discontinuity exists in the stratigraphy of the sample GAR-01 B (Fig. 2), and it was determined that the growing stalagmite was broken by visitors to the cave during the Middle Ages. The section of the sample representing stalagmite growth between 486 and 38 mm from top was broken off of GAR-01 B at 1.3 kyr (termed GAR-01 A and the subject of a future study) was found adjacent to GAR-01 B, and matches GAR-01 B petrographically, geometrically, and chronologically. Stalagmite GAR-01 therefore grew continuously from ∼14.0 kyr to the date of collection, and represents 80 cm of total growth with a

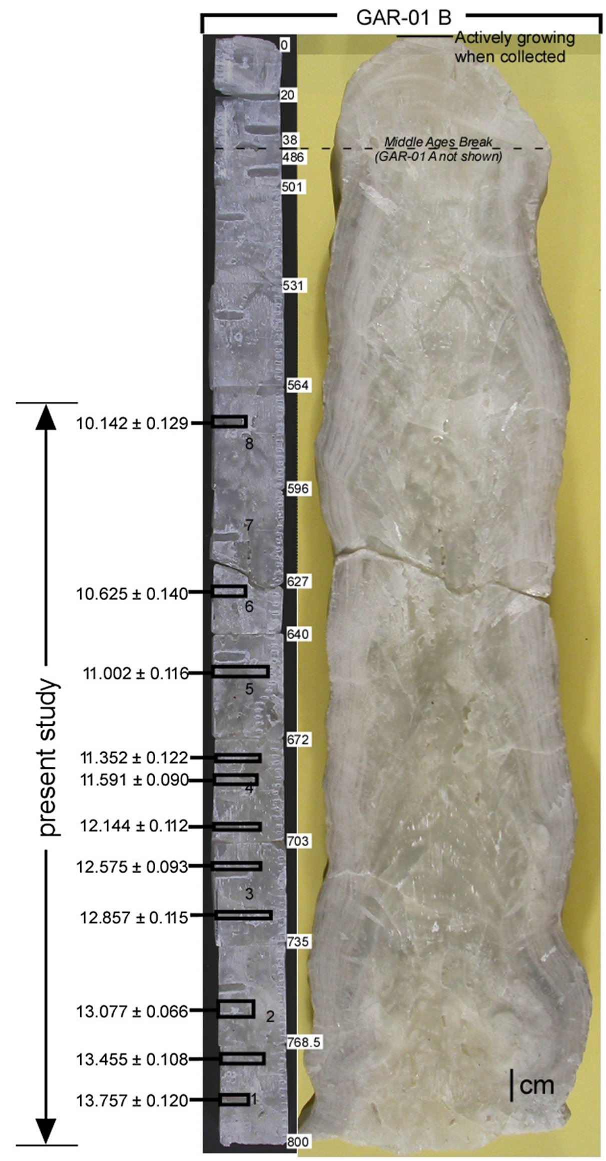

Fig. 2. Photograph of stalagmite GAR-01 B with U-series sample locations (black boxes) and corresponding ages (in years before 1950). For the present study, U-series powders were drilled at regular intervals across the lower 230 mm of GAR-01 B. U-series ages and 2σ errors are shown (also see Supplemental Table S1 for dating results). The location of the Middle Ages Break is shown by a dashed line but stalagmite GAR-01 A, discovered on the ground adjacent to the *in situ* portion of GAR-01 (GAR-01 B) in 2003, is not shown. White boxes provide absolute distance from top measurements in mm.

mean growth rate of 57 μm yr^{-1}. The present study focuses on the lower 230 mm of GAR-01 B growth and spans the Allerød to the Early Holocene.

For drill and laser isotope analysis, stalagmite GAR-01 B was sectioned along the central growth axis and polished to 1000 grit, then cut into 3 cm long slabs (in preparation for high-resolution microbeam stable isotope and trace element analysis) and cleaned in an ultrasonic bath of deionised water for 1 h. A conventional drill was used to extract powders at a mean resolution of 37 years for low resolution carbon and oxygen isotope analysis after which the slabs were analysed using a laser ablation–gas chromatography–isotope ratio mass spectrometry (LA-GC-IRMS) system at Royal Holloway University of London (RHUL), providing a mean resolution of 8.5 years. For laser trace element analysis, also conducted at RHUL (see Section 3.2), stalagmite slabs were re-polished using a diamond grinding disk to remove previous analysis tracks and cleaned for an additional two hours in a beaker of methanol placed in an ultrasonic bath.

3.2. Stable isotope and trace elemental analysis

The RHUL LA-GC-IRMS system uses a continuous helium flow sample chamber and a 25 W, 10.6 μm wavelength CO_2 laser heat source linked to a gas chromatograph (GC) and mass spectrometer (MS). 400-ms laser bursts (beam diameter, approximately 150 μm) produce CO_2 through thermal reaction; this CO_2 is then swept through an 80-cm packed GC column into the mass spectrometer for isotope analysis. Measurements are relative to a single reference gas injected at the start of each run. The $\delta^{18}O$ fractionation factor used is a function of ablation conditions accounted for through the use of solid standards. In the case of $\delta^{13}C$, there is no fractionation between calcite and ablation-generated CO_2. Replicate analyses of standards indicate that the isotope data are reproducible to better than 0.1‰ for $\delta^{13}C$ and 0.2‰ for $\delta^{18}O$. The data reproduce the features apparent from the low-resolution conventional drilling and conventional gas-source mass spectrometer (GV Instruments Multiflow-Isoprime systems at RHUL) analysis. Missing $\delta^{18}O$ data between 12.48 and 12.33 kyr are the result of the stalagmite slab chipping at the edge during laser ablation resulting in four spurious datapoints (both $\delta^{18}O$ and $\delta^{13}C$) that were subsequently deleted. For more details on the RHUL LA-GC-IRMS system see Spötl and Mattey (2006).

The high spatial resolution trace element datasets were obtained using a custom-designed excimer (193 nm; laser fluence ~4 J/cm^2) LA-ICPMS system at RHUL (RESOlution M-50 prototype coupled to an Agilent 7500ce quadrupole ICP-MS) that features a two-volume Laurin LA cell. Concentrations were determined for Na, Mg, Al, P, Ca, Cu, Zn, Rb, Sr, Y, Ba, Pb, and U, but only the concentrations of Mg, P, Ca, and Sr are discussed here. Stalagmite sections were analysed as continuous profiles using a rectangular spot (285 × 12 μm) which improves spatial resolution for layered samples more than fivefold relative to equivalent circular spots while maintaining high ICP-MS sensitivity. Profiles were analysed at 10 μm/s speed and a laser repetition rate of 15 Hz. The resultant spatial resolution is ~15 μm (equivalent to approximately a bi-monthly mean temporal resolution), however, considering our estimation of a 7.5 month dripwater residence time (Supplemental Fig. S3), the trace element data temporal resolution is subannual. Concentration quantification is based on ^{43}Ca as internal standard and NIST612 as external standard (Müller et al., 2009). A second trace element profile parallel but offset by 5 mm obtained across the YD interval during a separate LA-ICP-MS session replicates the original track (see Supplementary Material for additional information).

3.3. GAR-01 chronology

For the present study, eleven powder samples were drilled from distinct growth layers along the central axis of the lower 230 cm of the 800 mm long stalagmite using a handheld drill and a tungsten carbide drill bit. Chemical separation and purification of U–Th isotopes and analytical methods followed procedures outlined in Hoffmann et al. (2007) with samples analysed on a ThermoFinnigan Neptune multicollector inductively coupled mass spectrometer (MC-ICP-MS) at the University of Bristol. U concentrations range between 80 and 150 ng/g, ^{232}Th concentrations are between 0.02 and 0.6 ng/g indicating negligible to low detrital components in the samples. The $^{230}Th/^{232}Th$ activity ratio, which indicates the degree of detrital correction, varies between 22 and 2400. All ages were calculated using the half-lives reported in Cheng et al. (2000) and corrected for detrital contamination assuming a $^{238}U/^{232}Th$ activity ratio of 0.8±0.4 and a detrital component in U-series secular

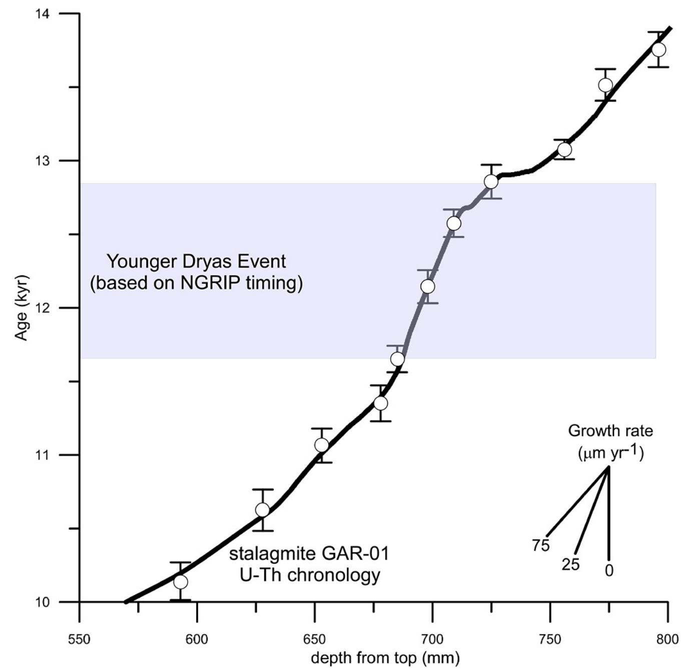

Fig. 3. U-series age model for the lower 230 mm of stalagmite GAR-01. GAR-01 U-series dates are plotted with 2σ error bars and the age model (black line) was calculated using the StalAge algorithm (Scholz and Hoffmann, 2011). The location of the YD based on NGRIP dates is illustrated by the shading, and growth rate based on the slope of the plotted age model is shown as an inset.

equilibrium (Wedepohl, 1995). Corrected and uncorrected results are given in Supplemental Table S1. All quoted uncertainties are at the 95% confidence level. The U–Th ages show that speleothem growth occurred between 0.5 and 14 kyr, and all twenty four dates from GAR-01 are in stratigraphic order along the growth axis. Initial $^{234}U/^{238}U$ activity ratios range between 1.125 and 1.155. U–Th dating was performed in several steps: first low spatial resolution dating results indicated that calcite precipitated during the YD phase is found between 680 and 730 mm from the top and subsequently high spatial resolution dating was done for the bottom 230 mm of the stalagmite to constrain timing and duration of the YD. A distance–age model was generated using the algorithm StalAge (Scholz and Hoffmann, 2011) and is very well constrained over the period of interest (Fig. 3).

Stalagmite GAR-01 grew continuously from 13.66 kyr to 2004 C.E., when it was collected based on 24$^{230}Th/U$ dates obtained along the length of the stalagmite (dating results above 570 mm from top to be presented in a future paper). Here we only discuss the record during and around the YD (from 14 to 10 kyr), which is constrained by 11$^{230}Th/U$ dates (Fig. 3 and Supplemental Table S1).

4. Results and discussion

4.1. Stable isotope ratios

A 3.1‰ shift in $\delta^{18}O$ to more negative values (the largest in the last 13.66 kyr) occurs between 12.90 and 12.65 kyr in GAR-01, consistent with the NGRIP ice core YD onset at 12.846 ± 0.138 kyr (Blockley et al., 2012; Rasmussen et al., 2006, 2014). This synchronicity suggests that GAR-01 $\delta^{18}O$ responded to regional scale (North Atlantic) air temperature cooling. Although several factors could have driven GAR-01 $\delta^{18}O$ variability, a plausible explanation is that YD-related temperature reductions across the North Atlantic were broadly synchronous (Figs. 4 and 5). Reduced air temperatures may have increased the cloud-base water vapour–meteoric precipitation fractionation factor, leading to lower meteoric precip-

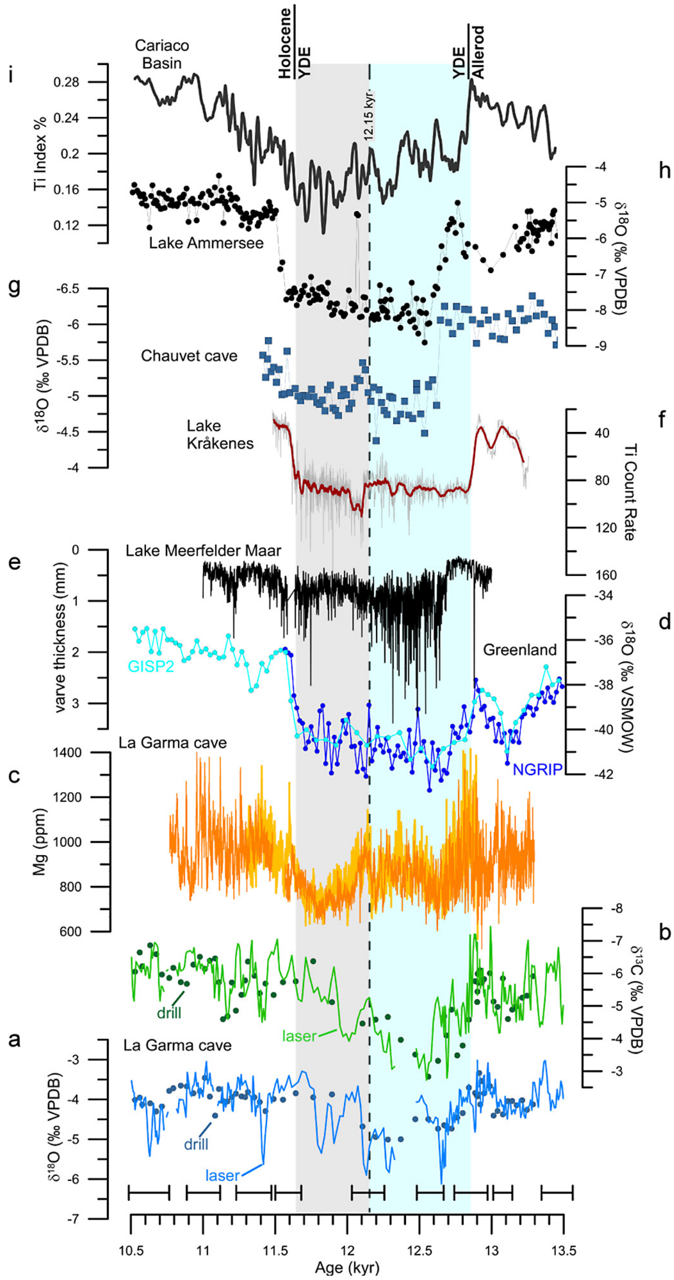

Fig. 4. Northern Hemisphere proxies of Younger Dryas conditions from the northern North Atlantic, mid-latitude Europe, and low latitude regions. (a) GAR-01 δ^{18}O laser ablation data (solid blue line) and conventional drill data (blue circles). The gap in the laser dataset between 12.33 and 12.48 ka is due to material lost during LA-ICP-MS analysis. (b) GAR-01 δ^{13}C laser ablation data (solid green line) and conventional drill data (large green circles). (c) GAR-01 Mg data original track (dark orange) and replicate track (light orange). (d) NGRIP and GISP2 δ^{18}O data (Steig et al., 1994). (e) MFM varve thickness data (Brauer et al., 2008). (f) LK Ti Count Rate (Bakke et al., 2009). The grey line is a three-point moving average. (g) Chauvet cave stalagmite δ^{18}O data (Genty et al., 2006). (h) Lake Ammersee ostracod δ^{18}O data (von Grafenstein et al., 1999). (i) Cariaco Basin Ti% index data (Haug et al., 2001). GAR-01 U-series dates obtained across the event are shown at the bottom of the diagram plotted with 2σ error bars. The vertical black dashed line highlights the '12.15 kyr event'. The turquoise and grey bars mark the timing of the YD according to NGRIP divided into the first and second stages of the event, respectively. (For interpretation of the references to colour in this figure legend, the reader is referred to the web version of this article.)

itation δ^{18}O (Rozanski et al., 1993) and consequently lower stalagmite calcite δ^{18}O. Although the abrupt temperature shift that marked the YD onset may have been accompanied by other effects (e.g. changes in moisture source δ^{18}O and moisture transport trajectories), the observed negative 3.1‰ shift suggests a reduction in temperature of 6–9 °C relative to Allerød temperatures (depending on assumptions regarding the slope of the rainfall δ^{18}O versus air temperature relationship). This interpretation is broadly consistent with independent terrestrial western European cooling estimates of 5–10 °C (Denton et al., 2005). A shift to drier conditions during the YD could not readily produce the observed shift to more negative δ^{18}O values, because the so-called 'amount effect' would produce shifts to heavier rather than lighter δ^{18}O based on the generally observed negative slope between rainfall δ^{18}O and amount (Rozanski et al., 1993) and the available Global Network of Isotopes in Precipitation (GNIP) data from the region (see Supplementary Material). On this basis, the lowest values for δ^{18}O in GAR-01 that occurred at 12.65 kyr are interpreted to reflect the coldest YD temperature in northern Iberia occurring synchronously with the lowest Greenland YD temperatures (12.65 kyr, NGRIP). Additionally, Iberian margin SST reconstructions (Bard, 2002) very closely track Greenland temperature throughout the Late Glacial and Holocene (Fig. 5), indicating that air temperatures in at least the Iberian coastal regions directly reflected North Atlantic conditions supporting our contention that shifts in GAR-01 δ^{18}O across the YD are largely a proxy for regional air temperature.

The timing and amplitude of δ^{18}O shifts in GAR-01 and the Candela stalagmite from El Pindal Cave (Moreno et al., 2010) located 70 km to the west of La Garma Cave further suggests that δ^{18}O in these records reflects regional climatic (temperature-induced isotope fractionation) rather than local or cave-specific hydrological routing effects (Fig. 5). The stalagmite δ^{18}O YD anomaly from Chauvet Cave (Genty et al., 2006) (southern France, 650 km to the east) is similar in structure and timing to our GAR-01 δ^{18}O record but the relationship with temperature is opposite (a decrease in δ^{18}O at 12.15 kyr was interpreted to reflect warming) (Fig. 4). The reasons for this apparent disparity between Chauvet Cave and the speleothem records from northern Spain remain unclear, but possible explanations are that the within-cave water–calcite precipitation fractionation factor (ca. $-0.24‰\,°C^{-1}$) exceeds the cloud-base vapour fractionation factor (Genty et al., 2006), or that the 'amount effect' was a more important factor at the more continental French site.

Approximately 50 years after the initial δ^{18}O shift in GAR-01, δ^{13}C exhibits a well-defined +4.5‰ anomaly (Fig. 4b) implying a lagged soil/ecosystem response to the initial climate forcing, a decrease in land surface bioproductivity, and/or a vegetation shift to a more cold/drought tolerant type, consistent with local pollen data that indicate a transition from temperate forest to herbaceous species in northern Iberia in response to drier and cooler conditions at this time (Moreno et al., 2010). Based on the GAR-01 δ^{18}O and δ^{13}C data, maximum YD cooling and ecosystem decline in northern Iberia occurred early within the YD, at approximately 12.7–12.5 kyr. This was followed by gradual warming and ecosystem recovery to pre-YD values at 11.65 kyr, again consistent with both regional and Greenland temperature reconstructions. This gradual temperature increase is punctuated with centennial-scale warming events, particularly at 11.68, 12.07, and 12.51 kyr, when northern Iberian temperature returned nearly back to Allerød values, before dropping back to lower YD values (Figs. 4 and 5).

4.2. High-resolution LA-ICPMS Mg data

Whereas the GAR-01 isotope data are interpreted to reflect the regional temperature (δ^{18}O) and local ecosystem (δ^{13}C) response to the YD (Figs. 4 and 5), the Mg dataset could in principle reflect several processes: a) various degrees of prior calcite precipitation (PCP) from the waters that fed stalagmite GAR-01, b) varying degrees of water–rock interaction, c) temperature via the temperature-sensitive Mg distribution coefficient in calcite (D_{mg}),

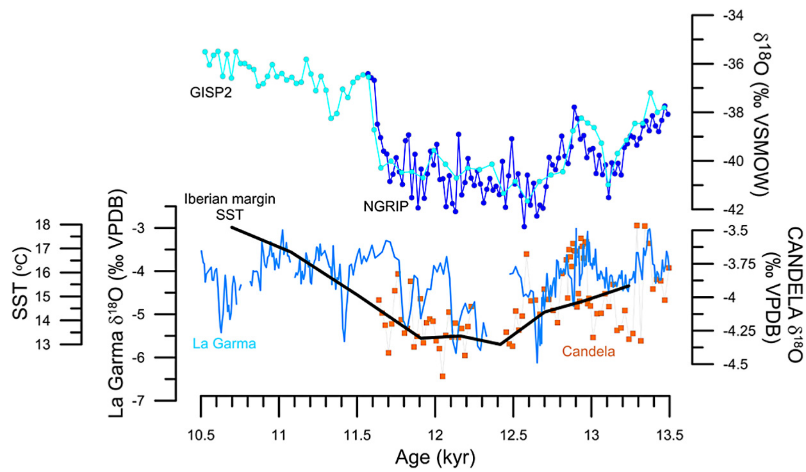

Fig. 5. Records proximal to La Garma Cave and those interpreted as reflecting regional temperature. The GAR-01 laser δ^{18}O record (blue), the Iberian margin SST record (black) (Bard, 2002), and the Candela stalagmite record from El Pindal Cave (orange squares) (Moreno et al., 2010) (lower panel) as well as Greenland ice core δ^{18}O records (Steig et al., 1994) (upper panel). (For interpretation of the references to colour in this figure legend, the reader is referred to the web version of this article.)

or d) varying marine aerosol contributions to the cave dripwater. Mg and Sr concentrations considered with δ^{13}C indicate that PCP did not significantly affect GAR-01 drip geochemistry. Mg concentrations decrease into the YD whereas δ^{13}C increases, and the process of PCP or increased bedrock interactions would have resulted in a positive, not negative, correlation ($r = -0.24$, $p < 0.01$ for the entire Mg–δ^{13}C relationship between 13.29 and 10.77 kyr based on Pearson's correlation analysis of the decadally-interpolated laser datasets). Although Mg and δ^{13}C are in fact correlated during the YD interval ($r = 0.26$, $p < 0.01$), the lack of a correlation elsewhere argues against a PCP control during this restricted interval as well. Furthermore, Mg and Sr do not plot along a PCP vector (Fig. 6), although this relationship is often not diagnostic because Sr incorporation is sensitive to competition and growth rate effects (Borsato et al., 2007; Sinclair et al., 2012). Increased groundwater residence times (and consequently increased bedrock contributions to the dripwater) would have produced a trend similar to PCP (Sinclair et al., 2012), and are similarly inconsistent with the observed Mg–Sr relationship (Fig. 6). Temperature, however, changed dramatically during the interval reconstructed, and would have affected D_{mg}. Based on the Iberian margin SST record (Bard, 2002) and the experimentally-derived D_{mg}–temperature relationship (Huang and Fairchild, 2001), the maximum possible shift in the GAR-01 Mg record attributable to temperature is a decrease of ~200 ppm, considerably less than the observed decrease of ~675 ppm from the Allerød to the coldest part of the YD. Consequently, although temperature change was undoubtedly a factor, it could not have been the dominant control on GAR-01 Mg concentrations over the YD. Importantly however, mean Mg and Sr concentrations for key intervals in GAR-01 do plot along a mixing curve constructed by calculating the Mg and Sr concentrations of hypothetical calcites in equilibrium with dripwater combined with variable marine aerosol contributions (Fig. 6), which is unsurprising given the cave site's proximity to the coast. The high-resolution GAR-01 Mg record is therefore interpreted as reflecting predominantly meteoric precipitation Mg concentrations (controlled largely by marine aerosol contributions) and to a lesser extent temperature through variations in (the temperature-dependent) D_{mg}. Currently, the strongest winds over northern Iberia are the westerlies, present predominantly during negative NAO phases. Marine aerosol emission rates are critically dependent on wind speed (Tsyro et al., 2011), and a logical consequence of this link is that the greatest amount of marine aerosol contributions to rainfall approximate westerly wind position (Tsyro et al., 2011). Importantly, research has already linked marine aerosol contribution amounts to NAO phase

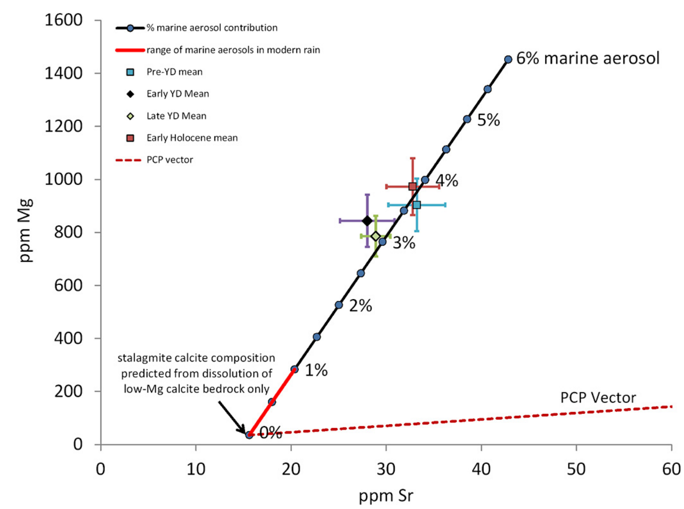

Fig. 6. Mean LA-ICP-MS Sr and Mg values for GAR-01 for the pre-YD (13.29 to 12.85 kyr), early YD (12.85 to 12.15 kyr), late YD (12.15 to 11.65 kyr), and, early Holocene (11.65 to 10.77 kyr) shown with error bars representing one standard deviation from the mean for each dataset. The solid line is a modelled calcite vector representing different amounts of marine aerosol contributions to the dripwater. The 0% marine aerosol contribution is defined as the Mg and Sr concentrations in calcite precipitated from a dripwater with Mg and Sr concentrations derived exclusively from the dissolution of the bedrock surrounding La Garma Cave. The Mg and Sr concentrations of seawater are derived from global averages (Chester, 1990). The percentages represent increasing percentage contribution of seawater to the dripwater (i.e., 0% = no seawater contribution, 5% = 5% of the dripwater is composed of seawater). These dripwater Mg and Sr values are then used to model the Mg and Sr values in calcite precipitated from this dripwater of varying marine aerosol contributions (the solid line), using the distribution coefficients given in Huang and Fairchild (2001). The range of marine aerosols found in modern rainfall was calculated using rainfall elemental concentrations compiled in Banasiek (2008) near Pindal Cave (70 km west of La Garma Cave) for a short interval from January 14, 2006 to February 26, 2007, and therefore may represent an underestimation of the total modern marine aerosol range possible. The samples were collected at a similar distance from the coast as La Garma.

(Hindar et al., 2004). In Norway for example, NAO positive phases are associated with a northward shift in westerly wind position, higher wind speeds, and greater marine aerosol (and specifically Mg) contributions to rainfall (Hindar et al., 2004). It is likely that westerly winds probably controlled past marine aerosol fluxes in rainfall as well; high aerosol contributions to the GAR-01 dripwater imply that the westerlies were positioned over the site, whereas reduced Mg fluxes suggest that the westerlies were positioned elsewhere. Based on elemental compositions in rainwater collected

70 km from La Garma, but approximately the same distance from the coast (Banasiek, 2008), modern marine aerosol contributions range up to 1%, well below the values of ~3.5% calculated here for the YD (Fig. 6). This difference likely reflects increased storminess during the late Glacial compared to current conditions (Fig. 6).

High amplitude, high frequency Mg variability between 12.9 and 12.15 kyr is interpreted to reflect alternating strong and weak westerlies over northern Iberia resulting from rapid north–south repositioning of the dominant westerlies, very similar to the wind reconstructions from MFM (at a slightly more northerly latitude) across the same time interval (Fig. 4). Decadal-scale oscillations within the GAR-01 Mg record during this early stage of the YD are those characteristic of the modern NAO, suggesting that a modern, NAO-like dipole mechanism controlled westerly track position during the first half of the YD. Because sea-ice extent is thought to largely control the position of the westerlies during this part of the Late Glacial (Brauer et al., 2008), we infer that sea-ice extent is oscillating on similar timescales. Existing sea-ice reconstructions for the North Atlantic based on the IP25 sea-ice proxy are too coarse to resolve sea-ice extent directly at that resolution (Müller and Stein, 2014; Pearce et al., 2013), so it is important to use other means, such as terrestrial wind records, to infer sea-ice extent indirectly. The frequency of Mg concentration fluctuations decreased from approximately ~10 years in the earliest YD to ~40 years between 12.3 and 12.15 kyr (Fig. 7b), possibly reflecting the reduced frequency of meridional westerly repositioning as a result of northward retreat and stabilisation of North Atlantic sea-ice extent toward the mid-YD. Mg concentration values peak within the YD at ~12.15 kyr, coincident with δ^{18}O excursions in the GAR-01, Greenland (Rasmussen et al., 2006), Chauvet cave (Genty et al., 2006) and Lake Ammersee (von Grafenstein et al., 1999) records that all imply rapid warming during the so-called '12.15 kyr event' (Figs. 4 and 7). The GAR-01 Mg data therefore suggest strong westerlies over La Garma during this interval coincident with warmer North Atlantic temperatures, implying that a lag existed between mid-YD warming and sea-ice collapse (i.e., warmer conditions should melt sea ice and redirect the westerlies to the north, but this did not occur immediately). After 12.15 kyr, a subsequent long-term and gradual northward displacement of westerly storm tracks from mid-latitude Europe to high-latitude Europe is implied by the Mg data and by previous reconstructions (Fig. 7) (Bakke et al., 2009; Brauer et al., 2008). However, this marked shift in westerly wind latitude precedes a major decrease in sea-ice extent inferred off of Newfoundland at 11.7 kyr (Pearce et al., 2013), suggesting that sea ice off of NW Europe retreated earlier than that off of North America, or that westerlies were shifting independently of sea ice. This pattern is consistent with previous coarsely resolved planktonic foraminifera based reconstructions that indicated a rapid northward sweeping retreat of the Polar Front along the eastern Atlantic Ocean margin compared with a more sluggish retreat along its western margin (Lowe et al., 1994; Ruddiman and Mcintyre, 1977). Our Mg data suggest steadily increasing contributions of marine aerosols starting from 11.8 kyr, interpreted as reflecting gradual migration of westerlies back to the south after reaching their most northerly position at that time. The GAR-01 data and our interpretations are consistent with the inferred northerly migration of the westerlies and Polar Front implied by central and northern European records at MFM and LK (Lane et al., 2013) and provides the first evidence from Iberia or lower latitude Europe to corroborate this previously inferred atmospheric repositioning.

4.3. Implications

The GAR-01 record supports the interpretations of the MFM and LK records from central and northern Europe (Bakke et al., 2009; Brauer et al., 2008; Lane et al., 2013), but provides a new perspective from an Atlantic margin site, proximal to the regions most affected by YD cooling (Shakun and Carlson, 2010). The timing of the initiation of Polar Front northward migration during the '12.15 kyr event' at the La Garma (43°N) site is also indistinguishable (i.e., within dating uncertainties) from that at the MFM (50°N) or LK (62°N) sites, supporting previous interpretations that the Polar Front retreated northward from its maximum southward extent at this time (Lane et al., 2013). However, the northward shift is much more abrupt in the latter two records (<20 years; Fig. 7) than at La Garma, where the westerly wind migration from the site took ~100 years to complete (Fig. 7b). This implies that meridional repositioning nearer the Atlantic occurred at a slower rate than further to the east in continental Europe, possibly linked to the effects of lingering North Atlantic sea ice compared to sea ice off Scandinavia and the influence of a freshwater cap distributed over the North Atlantic (Müller and Stein, 2014).

The new GAR-01 records provide information regarding both regional temperature (δ^{18}O) and Iberian wind strength (Mg) on a common timescale, and so can clarify the temporal relationships between the two parameters (Fig. 8). We propose that the westerlies reached their southernmost extent at some stage during the coldest part of the YD, possibly at around 12.15 kyr or just before, consistent with evidence of reduced wind strength at more northerly sites MFM and LK (Figs. 7 and 8). We suggest that the mean southernmost position of the westerlies may have been south of the La Garma site; the westerlies were still affecting northern Iberia at this time, but were too far south to influence MFM or LK significantly. At ~12.15 kyr, temperature begins to increase dramatically and is associated with a northward migration of westerlies that continued until ~11.8 kyr. Pearce et al. (2013) suggest that AMOC strengthening at approximately 12.3 kyr brought warmth to the North Atlantic, but that rapid sea-ice loss off the coast of Newfoundland and associated atmospheric circulation shifts was delayed until ~11.8 kyr. They suggest that the 12.3 kyr AMOC strengthening resulted in ITCZ shifts through a yet poorly-defined teleconnection, and then these ITCZ shifts were then propagated northward to higher latitudes via shifts in Hadley circulation cells and associated wind fields. Evidence from the high-resolution La Garma record broadly supports this interpretation, but the more southerly location of the westerlies implied by our record suggests that the AMOC strengthening did not affect atmospheric circulation considerably at ~12.3 kyr. Additionally, the northward migration of the westerlies and Polar Front implied by our record (at ~12.15 kyr) predates the break-up of sea ice off of Newfoundland proposed by Pearce et al. (2013) (at ~11.7 kyr), suggesting that sea ice loss occurred earlier off of NW Europe than off of North America. The GAR-01 record therefore suggests that regional warming occurred rapidly (at ~12.15 kyr) whereas shifts in atmospheric circulation were more gradual, more closely tracking the migration of the ITCZ (Figs. 7 and 8).

The sequence suggested by the GAR-01 data, considered with the other terrestrial wind records and marine sea-ice proxy records is: i) 12.85 to 12.3 kyr: westerlies fluctuating between northern Iberia and central Europe but moving to the south driven by progressively cooling temperatures and increasing sea ice extent, ii) 12.3 to 12.15 kyr: continued cold conditions; 'flickering' of westerlies over S Europe with northern Iberia near the far north of the range, iii) 12.15 kyr: rapid warming and loss of sea ice off of Scandinavia, abruptly redirecting westerly winds to northern Europe and Iberia, but with more pronounced northerly shifts further away from the Atlantic margin, iv) 12.15 to ~11.8 kyr: continued northward migration of westerlies across Europe, and v) 11.8 kyr: wholesale collapse of sea ice along the NW Atlantic Ocean adjacent to Newfoundland. This sequence suggests that sea-ice loss through the YD occurred gradually from east to west across the Atlantic over approximately 500 years.

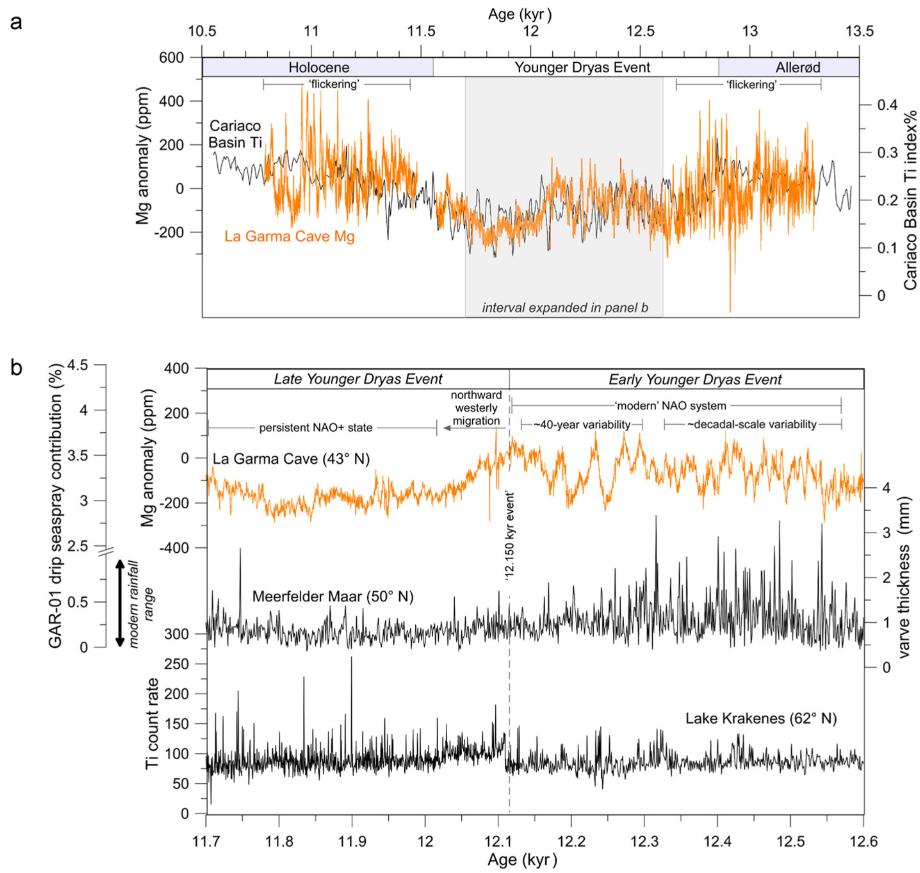

Fig. 7. The GAR-01 Mg compared to other low- and mid-latitude records. (a) The GAR-01 Mg (orange) and the Cariaco Basin (Haug et al., 2001) (black) records. The interval from 11.8 to 12.6 kyr for the GAR-01 Mg record is expanded in (b) and compared to the MFM (Brauer et al., 2008) and LK (Bakke et al., 2009) records. The dark double arrow to the left shows the modern % aerosol contribution near Pindal Cave (70 km west of La Garma Cave). The position of the vertical dashed line labelled '12.15 kyr event' was determined by the Garma, MFM and LK data and therefore lies between 12.15 and 12.1 kyr. (For interpretation of the references to colour in this figure legend, the reader is referred to the web version of this article.)

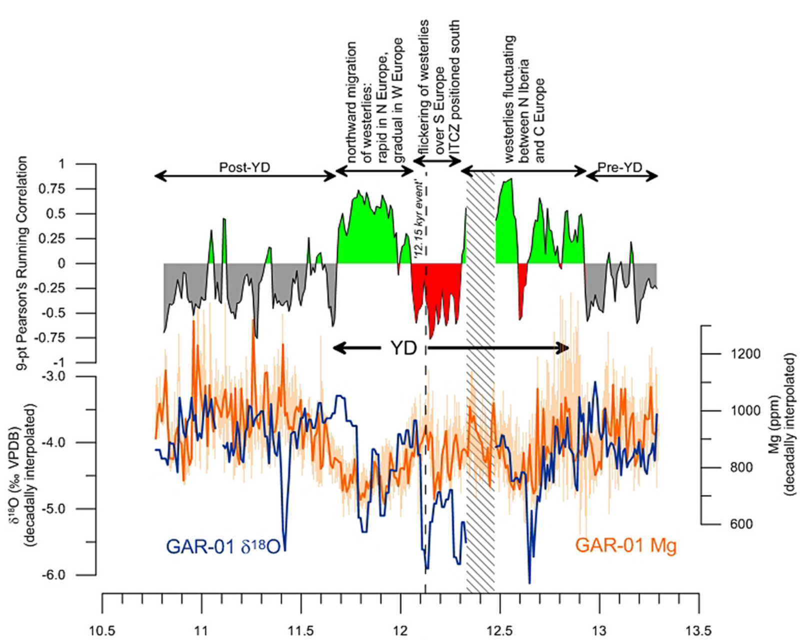

Fig. 8. The GAR-01 Mg (thick orange line) and the GAR-01 $\delta^{18}O$ record (thick blue line) regularly interpolated to be the same (decadal) resolution. Also shown is the uninterpolated GAR-01 Mg data with the original and replicate analysis track datasets combined (light orange line). A 9-pt Pearson's running correlation is shown (above) revealing intervals of positive (green) and negative (red) Mg–$\delta^{18}O$ correlation through the YD and primarily negative (grey) correlation during the pre- and post-YD. Black arrows at the top separate intervals of changing Mg–$\delta^{18}O$ correlation polarity and provide our interpretations. The YD time interval (12.85 to 11.65 kyr) is shown by the central black arrows. A four point $\delta^{18}O$ data gap that occurred (between 12.48 and 12.33 kyr) due to material loss during laser ablation analysis is identified by the hatched box. (For interpretation of the references to colour in this figure legend, the reader is referred to the web version of this article.)

5. Conclusions

The GAR-01 record reveals considerable interannual–decadal variability within the YD that is undetectable in lower resolution proxies. The GAR-01 Mg data are consistent with interpretations based on other high-resolution proxies from central and northern Europe constraining the latitude of the westerly winds, supporting the concept that a northerly migration of westerly wind position began at around 12.15, approximately halfway through the YD (Lane et al., 2013). However, the shifts observed at La Garma occurred over a longer timescale (between 12.1 and 11.8 kyr) than those inferred for LK and MFM, suggesting that Polar Front migration northward was spatially heterogeneous across Europe, and that the persistence of North Atlantic sea ice reduced the rate of westerly wind migration over northern Iberia compared to over central Europe. A correlation between inferred westerly wind position and the low latitude ITCZ corroborates previous research (Pearce et al., 2013) suggesting that strengthened AMOC resulted in gradual northward migration of the ITCZ and associated atmospheric circulation, including westerlies over Europe.

Our data further detail the nature of North Atlantic sea-ice loss during the YD and of the subsequent atmospheric reorganisation. Further research should focus on determining the exact nature of the AMOC/ITCZ teleconnection, to gain a better understanding of the interactions between North Atlantic sea ice extent and ITCZ migration on North Atlantic westerly wind position. A new high resolution archive of westerly wind variability from southern Europe would help constrain the precise location of the westerlies during the interval from 12.3 to 12.15 ka BP, when they may have been positioned south of northern Iberia. These results provide further evidence that substantial atmospheric circulation reorganisation can occur over just a few decades, leading to dramatic differences in local temperature, rainfall, and storminess. Previous research suggested that rapid climate change due to repositioned atmospheric circulation is often of greater local importance than climate change averaged over large geographic areas (e.g., Lane et al., 2013), and our high-resolution dataset from northern Iberia reinforces this concept.

Acknowledgements

This research was funded by Enterprise Ireland's Basic Research Grants Scheme and conducted in parallel with IF's Natural Environment Research Council (NERC) RAPID climate change programme funded ASCRIBE Project (Grant NER/T/S/2002/00448). FMcD acknowledges support from Science Foundation Ireland through Research Frontiers Grants 07/RFP/GEOF265 and 08/FRP/GEO1184. We thank Vanessa and Lorenzo Cociani for their assistance with an earlier version of this manuscript. The authors are also grateful to Colm O'Cofaigh, Wanda Stratford, and David Ashby for their assistance with Fig. 1a. Finally, we are grateful to Darrel Tremaine, Robert Jamieson, the ASCRIBE project researchers, and two anonymous reviewers for their helpful suggestions that greatly improved the manuscript.

Appendix A. Supplementary material

Supplementary material related to this article can be found online at http://dx.doi.org/10.1016/j.epsl.2015.03.015.

References

Arias, P., 2009. Rites in the dark? An evaluation of the current evidence for ritual areas at Magdalenian cave sites. World Archaeol. 41, 262–294.

Arias, P., Ontañón, R., 2012. La Garma (Spain): long-term human activity in a karst system. In: Skeates, K.A.B.a.R (Ed.), Caves in Context. The Cultural Significance of Caves and Rockshelters in Europe. Oxbow, Oxford, pp. 101–117.

Bakke, J., Lie, O., Heegaard, E., Dokken, T., Haug, G.H., Birks, H.H., Dulski, P., Nilsen, T., 2009. Rapid oceanic and atmospheric changes during the Younger Dryas cold period. Nat. Geosci. 2, 202–205.

Banasiek, A., 2008. The rain in Spain does not fall mainly on the plain: geochemical variation in cave dripwater and stalagmite records from Asturias, northern Spain, Geosciences. Williams College.

Bard, E., 2002. Abrupt climate changes over millennial time scales: climate shock. Phys. Today 55, 32–38.

Blockley, S.P.E., Lane, C.S., Hardiman, M., Rasmussen, S.O., Seierstad, I.K., Steffensen, J.P., Svensson, A., Lotter, A.F., Turney, C.S.M., Ramsey, C.B., 2012. Synchronisation of palaeoenvironmental records over the last 60,000 years, and an extended INTIMATE(1) event stratigraphy to 48,000 b2k. Quat. Sci. Rev. 36, 2–10.

Borsato, A., Frisia, S., Fairchild, I.J., Somogyi, A., Susini, J., 2007. Trace element distribution in annual stalagmite laminae mapped by micrometer-resolution X-ray fluorescence: implications for incorporation of environmentally significant species. Geochim. Cosmochim. Acta 71, 1494–1512.

Brauer, A., Haug, G.H., Dulski, P., Sigman, D.M., Negendank, J.F.W., 2008. An abrupt wind shift in western Europe at the onset of the Younger Dryas cold period. Nat. Geosci. 1, 520–523.

Broecker, W.S., 2006. Was the Younger Dryas triggered by a flood? Science 312, 1146–1148.

Broecker, W.S., Kennett, J.P., Flower, B.P., Teller, J.T., Trumbore, S., Bonani, G., Wolfli, W., 1989. Routing of meltwater from the Laurentide Ice-Sheet during the Younger Dryas cold episode. Nature 341, 318–321.

Carlson, A.E., Clark, P.U., Haley, B.A., Klinkhammer, G.P., Simmons, K., Brook, E.J., Meissner, K.J., 2007. Geochemical proxies of North American freshwater routing during the Younger Dryas cold event. Proc. Natl. Acad. Sci. USA 104, 6556–6561.

Cheng, H., Edwards, R.L., Hoff, J., Gallup, C.D., Richards, D.A., Asmerom, Y., 2000. The half-lives of uranium-234 and thorium-230. Chem. Geol. 169, 17–33.

Chester, R., 1990. Marine Geochemistry. Unwin Hyman, Boston.

Denton, G.H., Alley, R.B., Comer, G.C., Broecker, W.S., 2005. The role of seasonality in abrupt climate change. Quat. Sci. Rev. 24, 1159–1182.

Firestone, R.B., West, A., Kennett, J.P., Becker, L., Bunch, T.E., Revay, Z.S., Schultz, P.H., Belgya, T., Kennett, D.J., Erlandson, J.M., Dickenson, O.J., Goodyear, A.C., Harris, R.S., Howard, G.A., Kloosterman, J.B., Lechler, P., Mayewski, P.A., Montgomery, J., Poreda, R., Darrah, T., Hee, S.S.Q., Smitha, A.R., Stich, A., Topping, W., Wittke, J.H., Wolbach, W.S., 2007. Evidence for an extraterrestrial impact 12,900 years ago that contributed to the megafaunal extinctions and the Younger Dryas cooling. Proc. Natl. Acad. Sci. USA 104, 16016–16021.

Genty, D., Blamart, D., Ghaleb, B., Plagnes, V., Causse, C., Bakalowicz, M., Zouari, K., Chkir, N., Hellstrom, J., Wainer, K., Bourges, F., 2006. Timing and dynamics of the last deglaciation from European and North African δ^{13}C stalagmite profiles—comparison with Chinese and South Hemisphere stalagmites. Quat. Sci. Rev. 25, 2118–2142.

Gouveia, C., Trigo, R.M., DaCamara, C.C., Libonati, R., Pereira, J.M.C., 2008. The North Atlantic Oscillation and European vegetation dynamics. Int. J. Climatol. 28, 1835–1847.

Haug, G.H., Hughen, K.A., Sigman, D.M., Peterson, L.C., Rohl, U., 2001. Southward migration of the intertropical convergence zone through the Holocene. Science 293, 1304–1308.

Hindar, A., Torseth, K., Henriksen, A., Orsolini, Y., 2004. The significance of the North Atlantic Oscillation (NAO) for sea-salt episodes and acidification-related effects in Norwegian rivers. Environ. Sci. Technol. 38, 26–33.

Hoffmann, D.L., Prytulak, J., Richards, D.A., Elliott, T.R., Coath, C.D., Smart, P.L., Scholz, D., 2007. Procedures for accurate U and Th isotope measurements by high precision MC-ICPMS. Int. J. Mass Spectrom. Ion Process. 264, 97–109.

Huang, Y., Fairchild, I.J., 2001. Partitioning of Sr^{2+} and Mg^{2+} into calcite under karst-analogue experimental conditions. Geochim. Cosmochim. Acta 65, 47–62.

Kennett, D.J., Kennett, J.P., West, A., Mercer, C., Hee, S.S.Q., Bement, L., Bunch, T.E., Sellers, M., Wolbach, W.S., 2009. Nanodiamonds in the Younger Dryas boundary sediment layer. Science 323, 94.

Lane, C.S., Brauer, A., Blockley, S.P.E., Dulski, P., 2013. Volcanic ash reveals time-transgressive abrupt climate change during the Younger Dryas. Geology 41, 1251–1254.

Lowe, J.J., Ammann, B., Birks, H.H., Bjorck, S., Coope, G.R., Cwynar, L., Debeaulieu, J.L., Mott, R.J., Peteet, D.M., Walker, M.J.C., 1994. Climatic changes in areas adjacent to the North Atlantic during the last Glacial–Interglacial transition (14–9 ka BP) – a contribution to Igcp-253. J. Quat. Sci. 9, 185–198.

Moreno, A., Stoll, H., Jimenez-Sanchez, M., Cacho, I., Valero-Garces, B., Ito, E., Edwards, R.L., 2010. A speleothem record of glacial (25–11.6 kyr BP) rapid climatic changes from northern Iberian Peninsula. Glob. Planet. Change 71, 218–231.

Müller, J., Stein, R., 2014. High-resolution record of late glacial and deglacial sea ice changes in Fram Strait corroborates ice–ocean interactions during abrupt climate shifts. Earth Planet. Sci. Lett. 403, 446–455.

Müller, W., Shelley, M., Miller, P., Broude, S., 2009. Initial performance metrics of a new custom-designed ArF excimer LA-ICPMS system coupled to a two-volume laser-ablation cell. J. Anal. At. Spectrom. 24, 209–214.

O'Cofaigh, C., Dowdeswell, J.A., Jennings, A.E., Hogan, K.A., Kilfeather, A., Hiemstra, J.F., Noormets, R., Evans, J., McCarthy, D.J., Andrews, J.T., Lloyd, J.M., Moros, M., 2013. An extensive and dynamic ice sheet on the West Greenland shelf during the last glacial cycle. Geology 41, 219–222.

Pearce, C., Seidenkrantz, M.S., Kuijpers, A., Masse, G., Reynisson, N.F., Kristiansen, S.M., 2013. Ocean lead at the termination of the Younger Dryas cold spell. Nat. Commun. 4.
Pohlmann, H., Sienz, F., Latif, M., 2006. Influence of the multidecadal Atlantic meridional overturning circulation variability on European climate. J. Climate 19, 6062–6067.
Rasmussen, S.O., Anderson, K.K., Svensson, A.M., Steffensen, J.P., Vinther, B.M., Clausen, H.B., Siggard-Andersen, M.-L., Johnsen, S.J., Larsen, L.B., Dahl-Jensen, D., Bigler, M., Rothlisberger, R., Fischer, H., Goto-Azuma, K., Hansson, M.E., Ruth, U., 2006. A new Greenland ice core chronology for the last glacial termination. J. Geophys. Res. 111, D06102. http://dx.doi.org/10.1029/2005JD006079.
Rasmussen, S.O., Bigler, M., Blockley, S.P., Blunier, T., Buchardt, S.L., Clausen, H.B., Cvijanovic, I., Dahl-Jensen, D., Johnsen, S.J., Fischer, H., Gkinis, V., Guillevic, M., Hoek, W.Z., Lowe, J.J., Pedro, J.B., Popp, T., Seierstad, I.K., Steffensen, J.P., Svensson, A.M., Vallelonga, P., Vinther, B.M., Walker, M.J.C., Wheatley, J.J., Winstrup, M., 2014. A stratigraphic framework for abrupt climatic changes during the Last Glacial period based on three synchronized Greenland ice-core records: refining and extending the INTIMATE event stratigraphy. Quat. Sci. Rev. 106, 14–28.
Rozanski, K., Araguas-Araguas, L., Gonfiantini, R., 1993. Isotopic patterns in modern global precipitation. In: Swart, P.K., Lohmann, K.C., McKenzie, J., Savin, S. (Eds.), Climate Change in Continental Isotopic Records. American Geophysical Union, Washington, DC, pp. 1–36.
Ruddiman, W.F., Mcintyre, A., 1977. Late Quaternary surface ocean kinematics and climatic change in the high-latitude North Atlantic. J. Geophys. Res. 82, 3877–3887.
Ruddiman, W.F., Mcintyre, A., 1981. The North-Atlantic Ocean during the last deglaciation. Palaeogeogr. Palaeoclimatol. Palaeoecol. 35, 145–214.
Rudzka-Phillips, D., McDermott, F., Jackson, A., Fleitmann, D., 2013. Inverse modelling of the C-14 bomb pulse in stalagmites to constrain the dynamics of soil carbon cycling at selected European cave sites. Geochim. Cosmochim. Acta 112, 32–51.
Scholz, D., Hoffmann, D.L., 2011. StalAge – an algorithm designed for construction of speleothem age models. Quat. Geochronol. 6, 369–382.
Shakun, J.D., Carlson, A.E., 2010. A global perspective on Last Glacial Maximum to Holocene climate change. Quat. Sci. Rev. 29, 1801–1816.
Sinclair, D.J., Banner, J.L., Taylor, F.W., Partin, J., Jenson, J., Mylroie, J., Goddard, E., Quinn, T., Jocson, J., Miklavic, B., 2012. Magnesium and strontium systematics in tropical speleothems from the Western Pacific. Chem. Geol. 294.
Souza, P., Cavalcanti, I.F.A., 2009. Atmospheric centres of action associated with the Atlantic ITCZ position. Int. J. Climatol. 29, 2091–2105.
Spötl, C., Mattey, D.P., 2006. Stable isotope microsampling of speleothems for palaeoenvironmental studies: a comparison of microdrill, micromill and laser ablation techniques. Chem. Geol. 235, 48–58.
Steig, E.J., Grootes, P.M., Stuiver, M., 1994. Seasonal precipitation timing and ice core records. Science 266, 1885–1886.
Tsyro, S., Aas, W., Soares, J., Sofiev, M., Berge, H., Spindler, G., 2011. Modelling of sea salt concentrations over Europe: key uncertainties and comparison with observations. Atmos. Chem. Phys. 11, 10367–10388.
von Grafenstein, U., Erlenkeuser, H., Brauer, A., Jouzel, J., Johnsen, S., 1999. A mid-European decadal isotope-climate record from 15,500 to 5000 years B.P. Science 284, 1654–1657.
Wedepohl, K.H., 1995. The composition of the continental-crust. Geochim. Cosmochim. Acta 59, 1217–1232.
Young, N.E., Briner, J.P., Rood, D.H., Finkel, R.C., 2012. Glacier extent during the Younger Dryas and 8.2-ka event on Baffin Island, Arctic Canada. Science 337, 1330–1333.